Synthesis, Mechanical and Tribological Characteristics of Immiscible Alloys

SANJAY SRIVASTAVA

Materials Science & Metallurgical Engineering
Maulana Azad National Institute of Technology, Bhopal-462051(India)
Email: s.srivastava.msme@gmail.com

Abstract- A modified impeller mixing coupled with chill casting technique was used for the preparation of immiscible alloys. In this paper Al-Fe binary alloys was chosen for this study. This binary system shows the miscibility gap at specified concentration and temperature. The electrolytic grade iron powder of 300mesh size was dispersed in the melt of commercially pure aluminum. The iron content in the composite varied from 1.67 to 11.2 wt%. Experimental quantitative expressions, which correlate UTS, yield tensile strength, elongation, wear volume and frictional coefficients to the presence of iron in the matrix, have been determined. The presence of iron in the composite improved the ultimate tensile strength, 0.2% proof stress and the hardness. The ductility showed the adverse effect with increase of the iron content in the matrix. The results from microstructure showed the presence of second phase particles at the grain boundaries of aluminum-rich phase as well as within the grain itself which was confirmed by EPMA line as well as XRD analysis. The experimental data refer to correlation with the directional transient solidification of hypereutectic Al-Fe alloys and the percentage of the iron in the matrix. These composite have also been subjected to wear and friction testing at different operating parameters. The XRD analysis was used to analyze the wear debris.

Index Terms- Al-Fe composite, Liquid Metallurgy, Wear, Friction, Worn surface

I. INTRODUCTION

There are a number of elements which are not soluble in the aluminum matrix. These elements may be either soft element or hard elements, depends upon the nature of the elements taken. They exhibit two immiscible liquid phases within a certain temperature range. However, the different density of these liquid phases leads, to the formation of two layers. This prevents the homogeneous distribution of particles in a matrix using simple and inexpensive casting processes. Therefore, the industrial exploitation of such alloys has also been limited so far. Immiscible alloys have been studied intensively for the last decades, mainly focusing on two aspects: the fundamental mechanism of secondary phase segregation/coarsening; and mixing approaches for the fabrication process. The development of immiscible alloys has been largely constrained by the conventional equilibrium processing, which generally results in gross segregation due to the wide miscibility gap, and high disparity in the densities and melting temperatures between the immiscible elements1. For example, aluminum alloys with proper distribution of lead have potential as materials for plain bearings, because of the lubrication ability of lead in the aluminum matrix 2. However, owing to the immiscibility of lead phase in the Al matrix 3 the grossly segregated lead may sometimes act as a kind of inclusion.

The idea is to obtain aluminum matrix with finely distributed particles of e.g. indium, bismuth or lead as a soft phase or iron, nickel or cobalt as a hard phase with lubricating function. However this is still far from the practical application because the miscibility phenomenon poses problems during solidification 4-5. A miscible gap in the liquid state is found in metal-metal systems such as Al-Bi, Al-Pb, Cu-Pb, Zn-Pb, Ga-Pb 6 etc. A typical equilibrium phase diagram is shown in Figure1. By means of a rapid solidification technique, Al-based (Al–In Pb Sn Cd) 7-8 and Cu-based (Cu–Pb, Cu–Pb–Sn) alloys have been synthesized with uniform distributions of the fine immiscible particles embedded in the matrix, indicating that the microstructure could be considerably refined compared with conventionally processed materials. Similar to rapid solidification, ball-milling is another effective nonequilibrium process for producing novel materials 9. Both Cu-Fe and Cu-V alloy system have significantly asymmetric phase diagram.

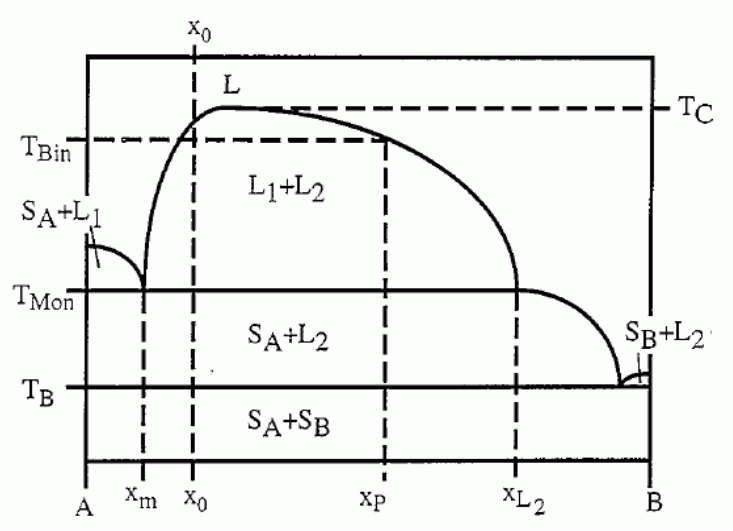

Figure 1: Typical binary phase diagram with a miscible gap in the liquid state

In addition, the cohesive energy of the solvent and solute atoms are also different, so that Cu atom mobility in Fe matrix is different from Fe mobility in Cu matrix, and the same thing happens for the Cu-V alloy10. Al–Fe alloys are attractive for applications at temperatures beyond those normally associated with the conventional aluminum alloys. Alloying Al with Fe increases the high temperature strength due to the dispersion of second phase particles.

Unfortunately, the equilibrium solubility of Fe in the Al lattice is very low, and it does not exceed 0·03%. Two points are to be noted: (1) the solubility of Fe in Al is extremely small; only 0.04 wt% Fe at 655oC and decreasing to virtually zero at room temperature; and (2) the second equilibrium eutectic phase is the intermetallic phase FeAl3 as shown in Figure 2. The miscibility gap is found between the variable percentages of aluminum. Hence, these alloys cannot be precipitation strengthened by conventional ageing treatments 11. The strengthening effect can be enhanced by increasing the solid solubility of Fe in the Al matrix by some nonequilibrium processing techniques, viz. rapid solidification processing (RSP) 9, 12-14 mechanical alloying (MA) 15-19 and severe plastic deformation (SPD)7.

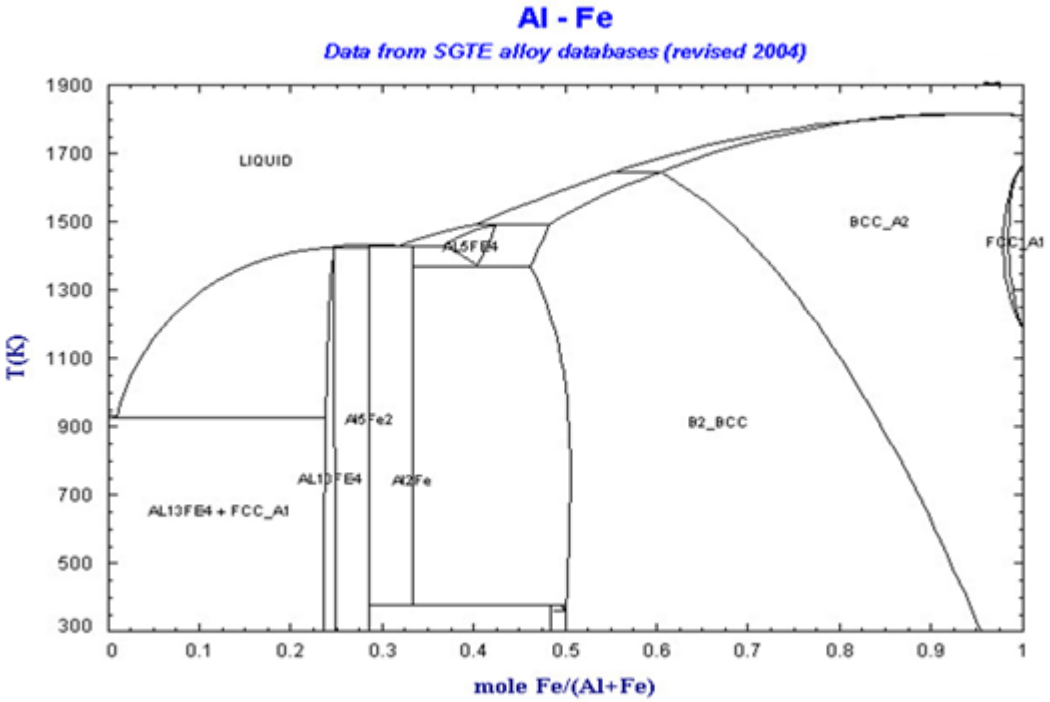

Figure 2: Typical Al-Fe phase diagram

The focus has increasingly shifted toward discontinuously-reinforced composites as a competition to continuous fibre reinforced composites from the standpoint of isotropic mechanical properties [20-26]. PMMCs have been shown to offer improvements in strength, wear resistance, structural efficiency, reliability, and control of physical properties such as density and coefficient of thermal expansion [26]. The strength of PMMCs increases with decreasing reinforcement size, however the fine size and larger volume fractions lead to severe agglomeration of the discontinuous reinforcement.

The study of the tribological behavior of materials can bring important contributions to fuel consumption reduction and to damage prevention during the service of components and equipment [27]. Rao et al. [28] state that the strain-hardening tendency of Al-Si alloys depends on the DAS and that the size of the eutectic silicon governs the wear behavior of these alloys. Kori et al. [29] studied the influence of the grain refiner on the wear resistance of as-cast Al-Si alloys and found that the reduction of the DAS improves the wear resistance due to both the production of more homogenously distributed Si particles and the refinement of these particles [30].

The present article aims to contribute to better understanding of the interrelation between presence of the hard particles in the matrix and the corresponding mechanical properties and wear behavior.In the present work, Al-Fe composites are being produced by liquid metallurgical route.

II. Experimental Preparation of Al-Fe Composite

Selection of materials and procedure for preparation

Commercially pure aluminum (99.8%), electrolytic iron powder of 50 μm size was selected for the preparation of Al-Fe composites with different compositions.

The experimental setup used for mixing and casting of composites is shown in Figure 3. It comprises of a cylindrical sillimanite crucible of 150mm diameter and 250mm depth with attachment of four baffles to its sidewalls for proper dispersion of second phase in melt during stirring. The crucible was placed in

an electric heated muffle furnace. It was also equipped with a bottom pouring attachment, which could be closed or opened by graphite stopper with a lever system.

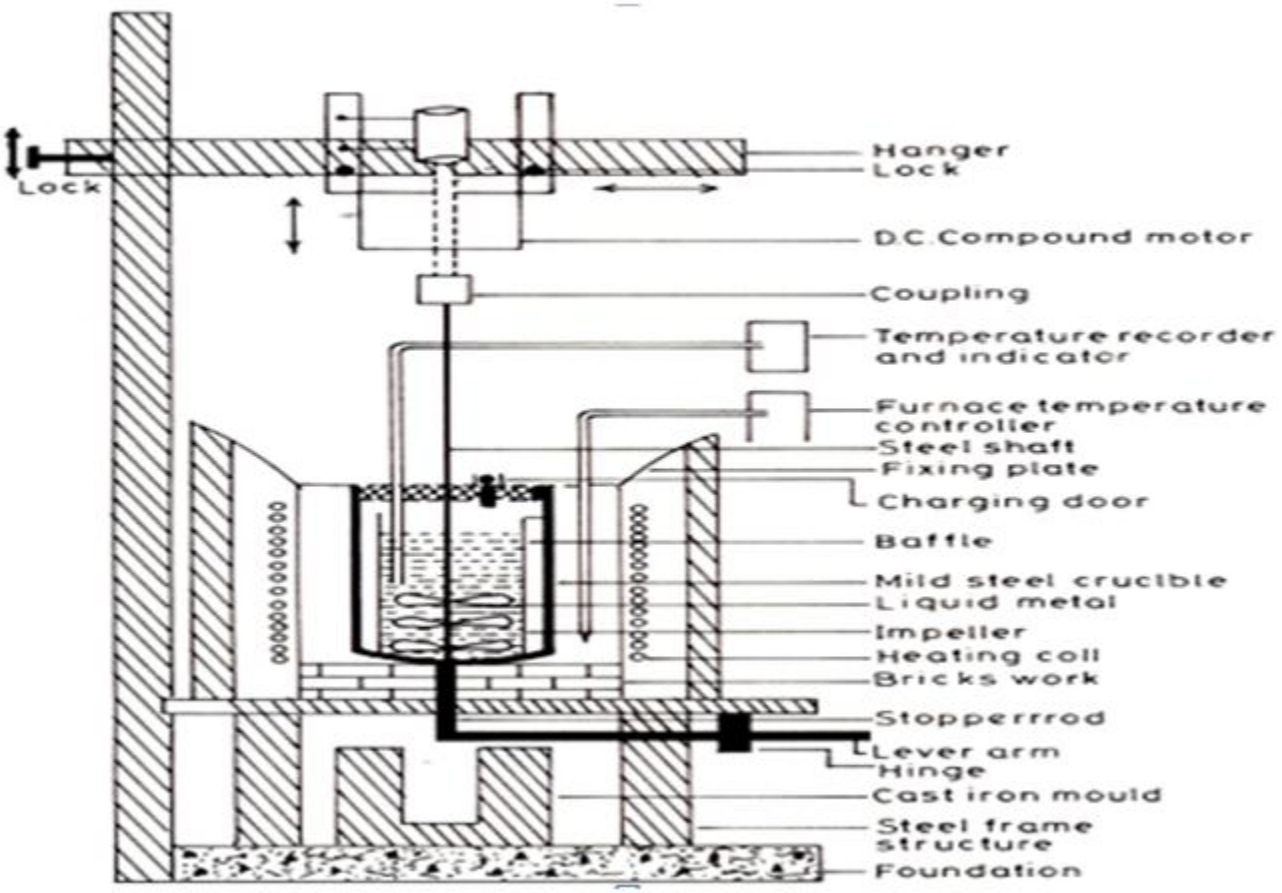

Figure 3: Schematic diagram of casting set-up

A steel mould was placed beneath the furnace to cast the molten metal. In the top cover suitable opening was provided to charge materials and insert thermocouples. The temperature of the furnace could be controlled with an accuracy of about $\pm 5^0$C. Metallic bath temperature was measured continuously by chromel/alumel thermocouple. The agitator system could be raised or lowered with the help of the hanger and steel frame structure. After adjusting the mixer in a central position and required height from the bottom of the crucible, the motor was bolted and locked while mixing of melt. Three-blade impeller was used for effective mixing. This design provides very high rates of shear and only axial and radial flow currents are utilized for mixing without any significant vortex formation due to the presence of baffles. The Al-Fe composites were prepared employing liquid metallurgical route. The required amount of commercial pure aluminum was charged into the crucible and aluminum was heated to a temperature 200^0C above its melting point i.e. 662^0C. A mechanical stirrer was inserted into the melt, and agitation was started at a speed of 35 rotations per second. The 50-µm-size electrolytic grade iron powder was charged into the melt during stirring and the addition of the particulate into the melt was facilitated by vortex created by stirring action. Mixing was done for a period of 60 seconds. The emulsion was poured into the chilled cylindrical mould placed beneath the crucible. The same procedure was adopted for different compositions. Cylindrical casting of length 20cm and dia.2cm were obtained.

Evaluation of as-cast Properties of the Composite

The wet chemical analysis was used to determine the percentage of iron in the bulk. The EDAX analysis was done as a confirmation test to iron presence. EPMA has been used to trace out the presence of iron which is either present at the grain boundary or within the grain of the composite. X-ray diffraction analysis was carried out for phase analysis.

The metallographic specimens were prepared using standard technique and studied under SEM for different feature present. The densities of the composite were determined using Archimedie's principle. The hardness of the entire composite was measured using a Vickers hardness testing machine. The hardness was measured using Vickers hardness instrument Leitz Welzlar at a load of 49N. At least 3 indentations have been taken for each point. Tensile testing of all the Al-Fe composite was performed stress along with percentage elongation and reductions in area were computed from the results. During tensile

testing evaluation of the composite materials, the strain rate was kept $2.5s^{-1}$.

Wear test

A pin-on-ring configuration utilized in earlier studies was used to simulate the sliding wear behavior between the sheave wheel and cable. A pin on disc apparatus Figure 4 was used to investigate the dry sliding wear characteristics of the aluminium alloy and the composites. The cylindrical test pin of 10 mm diameter and 40mm length were used against a hardened steel disc of 120 mm diameter.

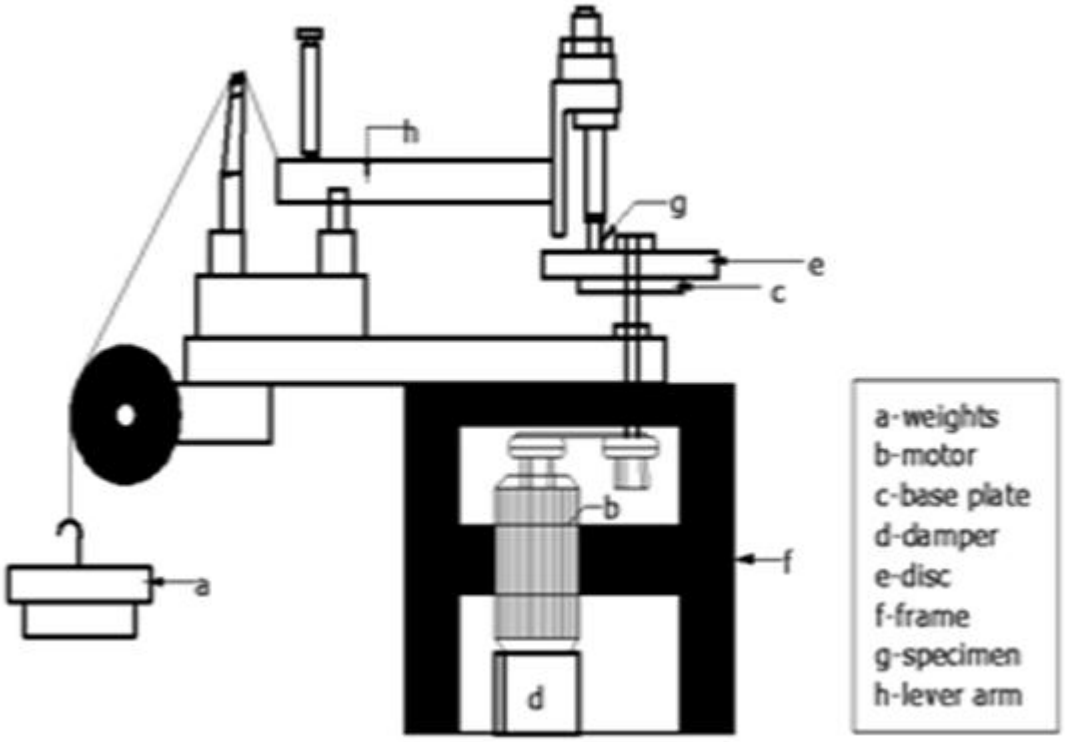

Figure 4: Schematic of pin on disc wears taking apparatus

Wear specimens of 10 mm diameter and 40 mm height were cut from as cast samples and machined and polished for wear test. Wear tests were conducted with a variable applied pressure of 14 Mpa and a sliding speed of 0.5 m/s with a constant sliding distance of 2500 meters. Wear test were also conducted with selected varying speeds and sliding distance ranging up to 40000 meters. The initial weight of the specimen was determined in a digital balance with a precision of ± 0.1 mg. The pin was kept pressed against a rotating steel disc of hardness 58 HRc under loaded condition.

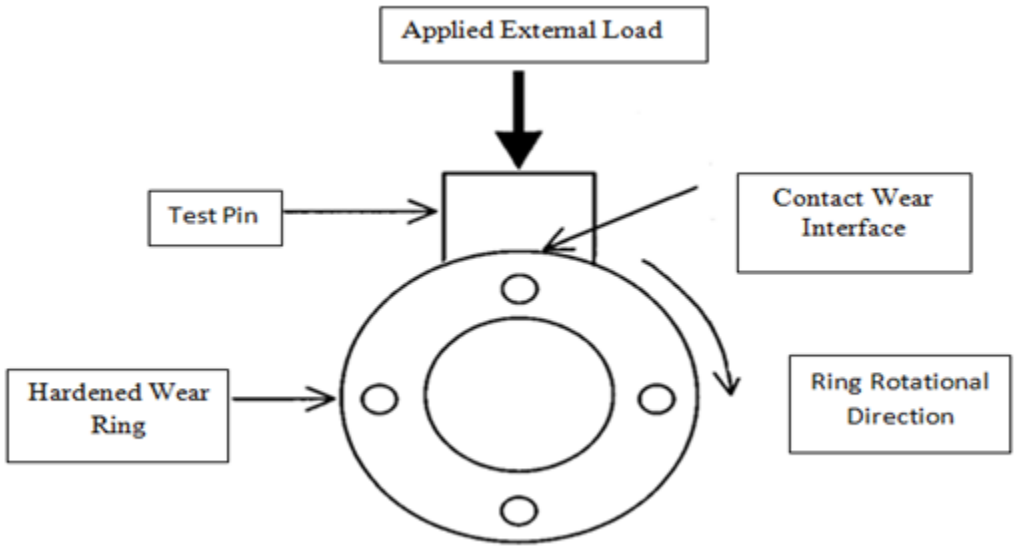

Figure 5: Pin-on-ring configuration used to evaluate the sliding wear resistance of the candidate materials and coatings

Figure 5 shows the basic pin-on-ring configuration used with the pneumatically loaded pin forced onto the rotating ring. During the sliding wear tests, an initial wear-in period was used to allow the pin to conform to the curved surface of the ring as shown in the figure. Since the ring was rotated at a constant speed, the total sliding distance was calculated from knowledge of the ring diameter (12 cm) and the test duration of the pins in contact with the steel disk. The length of contact time between the pin and disk varied depending on the time required before the onset of chattering. Lubrication was not used during any of the wear tests conducted during this study. Before each wear test, the dimensions of the pins were carefully measured to calculate the exact surface area and corresponding load required to maintain a desired interfacial nominal pressure of 13.9 Mpa. However, all pins had a pre-wear surface area (apparent) of approximately 0.32 cm^2. It was determined that the increase in surface area of the pins after conforming to the wear surface on the ring was negligible due to the relatively large wear ring diameter.

On completion of the running through the required sliding distance the specimen pins were cleaned with acetone, dried and their weight were again determined for ascertaining the weight loss. After each wearing interval, the pin was cleaned, weighed, and then positioned back in the wear tester for another wear interval. After sufficient data were collected for a particular pin and linearity established, the wear ring was re-ground to remove any adhered materials. If it was the last run for a particular pin, a new ring was implemented for the next series of tests. The frictional traction encountered by the pin in sliding is measured by a PC based data logging system. Tribological testing was conducted at varying sliding distances, applied loads and sliding velocities. In this experiment, the velocities were varied from 0.732m/sec to 3.82 m/sec and the loads were varying from 9.8N to 49N.

III. Result and Discussion

Chemical Analysis

Volumetric method is one of the most versatile techniques for the determination of element present at the microscopic level. In Al-Fe composites, iron is the minor constituent phase. Its percentage is determined by using the volumetric titration method. Specimens from different sections were used to find out the uniformity of dispersion and results are tabulated in Table 1. Further to confirm the presence of iron in the composites, energy depressive X-ray analysis (EDAX) was also used. Figure 6 and 7 shows the EDAX monographs of composite with two different compositions. In these monographs larger peaks correspond to aluminum and smaller ones to iron. It confirms the presence of iron in the Al-Fe composite. The results were also confirmed with EPMA and EDAX analysis.

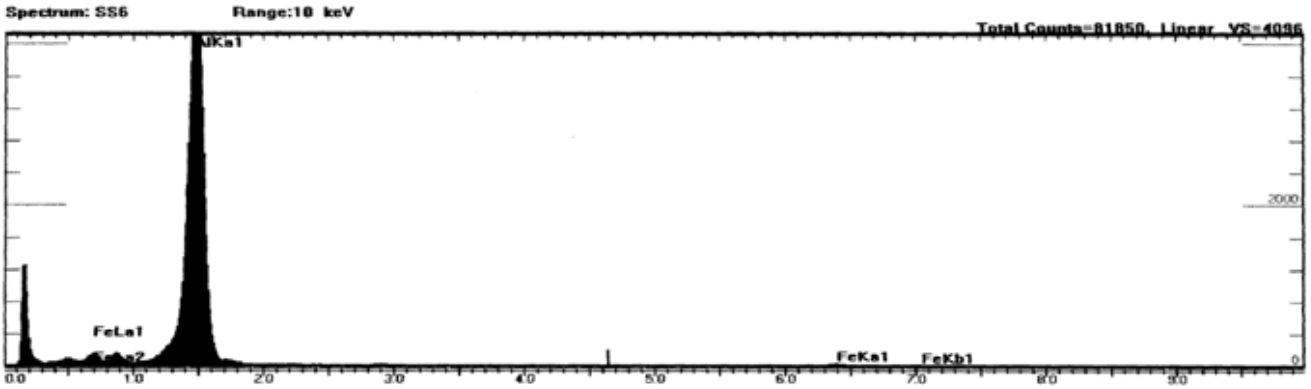

Figure 6: EDAX monograph of Al-6.23%Fe composite

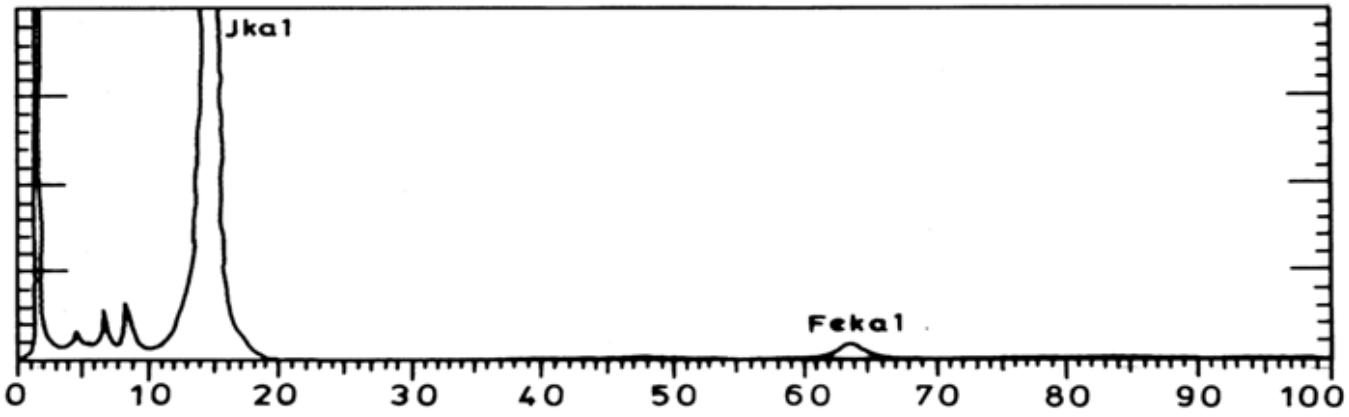

Figure7: EDAX monograph of Al-11.2%Fe composite

Physical and Mechanical analysis

Tables 1 show the physical properties of the different Al-Fe composites. It is observed from the table that the density increased from 2.79 to 3.08 as the iron content varied from 6.32 to 11.2%. The mechanical properties of the composites are tabulated in Table 2. There is slight increase in the ultimate tensile strength (142 to 184MPa) 0.2% off-tensile stress (59 to 83MPa) as the iron content increased from 1.67 to 11.2% wt in the composite, providing a strengthening effect. However percentage elongation decreased from 32 to 17 with increase in the iron from 1.67 to 11.2wt. %. Table 2 also shows the hardness values for all the four composites with different compositions. Hardness of the composites increases from 95 to 179 with increase in iron content from 1.67 to 11.2%. The mechanical properties of cast aluminum are adversely affected by the presence of iron as large primary or pseudo-primary crystals [31, 32].

Metallographic Analysis

Figure 8 (a) to (d) show the optical micrographs of composites with 1.67 to 11.2%Fe at same magnifications. These figures clearly reveal the presence of larger amount of second phase particles. These second phase particle exist in the elongated form.

Table 1. Chemical composition and Physical properties of Al-Fe composites

Composite	wt.% Fe	wt.% Al	Density (Theoretical) g/cm^3	Density (Experimental) g/cm^3
Al-1.67% Fe	**1.67**	**Remainder**	**2.79**	**2.63**

Al-3.36% Fe	**3.36**	**-do-**	**2.84**	**2.65**
Al-6.23%Fe	**6.23**	**-do-**	**2.96**	**2.79**
Al-11.2%Fe	**11.2**	**-do-**	**3.28**	**3.08**

Table 2: Mechanical properties of the Al-Fe composite

Composite	**HV**	**UTS (MPa)**	**0.2%PS (MPa)**	**Elongation (%)**
Al-1.67% Fe	**95**	**142**	**59**	**32**
Al-3.36% Fe	**131**	**153**	**70**	**30**
Al-6.23%Fe	**163**	**159**	**74**	**27**
Al-11.2%Fe	**179**	**184**	**83**	**17**

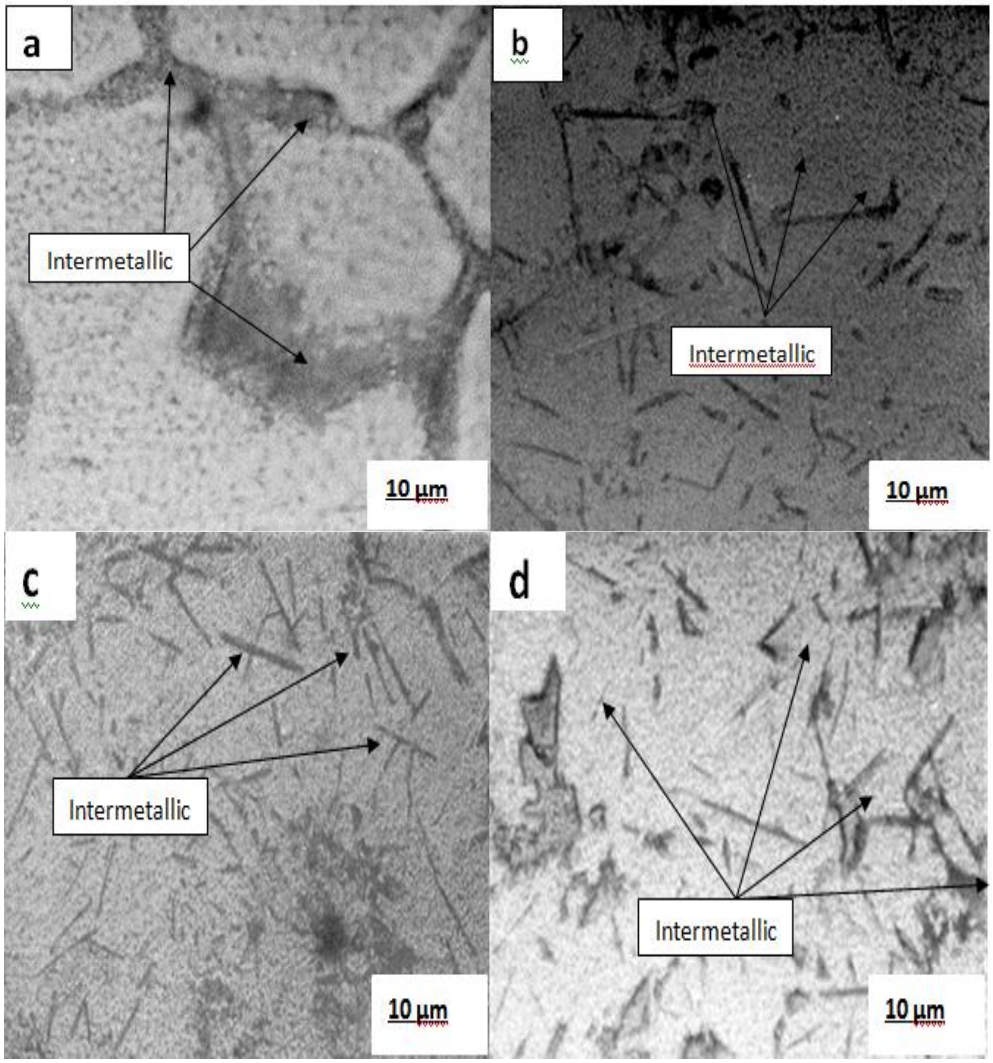

Figure 8: Optical micrographs of (a) Al-1.67%Fe (b) Al-3.36%Fe (c) Al-6.23%Fe (d) Al- 11.2% Fe composite

These elongated forms appear in the needle shape at higher magnification and at the higher percentage of iron content. The needle shape intermetallic increases with increasing iron content. All the composites were also studied under SEM for further investigation of the microstructures. Figure 9 a to d shows the SEM micrographs of all the composites. At the lower magnification, clusters of Al-Fe intermetallics were seen, but at the high magnification (only given at the higher magnification), needle shape intermetallics were clearly visible.

XRD analysis was conducted for all the four compositions produced with different iron percentage. These composite were fabricated by chill casting methods. The iron particles are uniformly distributed within the matrix by sudden cooling. XRD monographs for different compositions are shown in Figure 10 a to d for all composition of the selected composite materials.

In these curves large peaks correspond to major phase aluminum and smaller one corresponds to $FeAl_3$ [24, 33]. Analysis of the Al – Fe composite materials fabricated from liquid metallurgy methods, the prepared system (i.e., composite materials) bearing 0.3 – 1.5 at.% Fe has shown that their structure is represented by a supersaturated solid solution of iron in aluminum, which decomposes after heat treatment

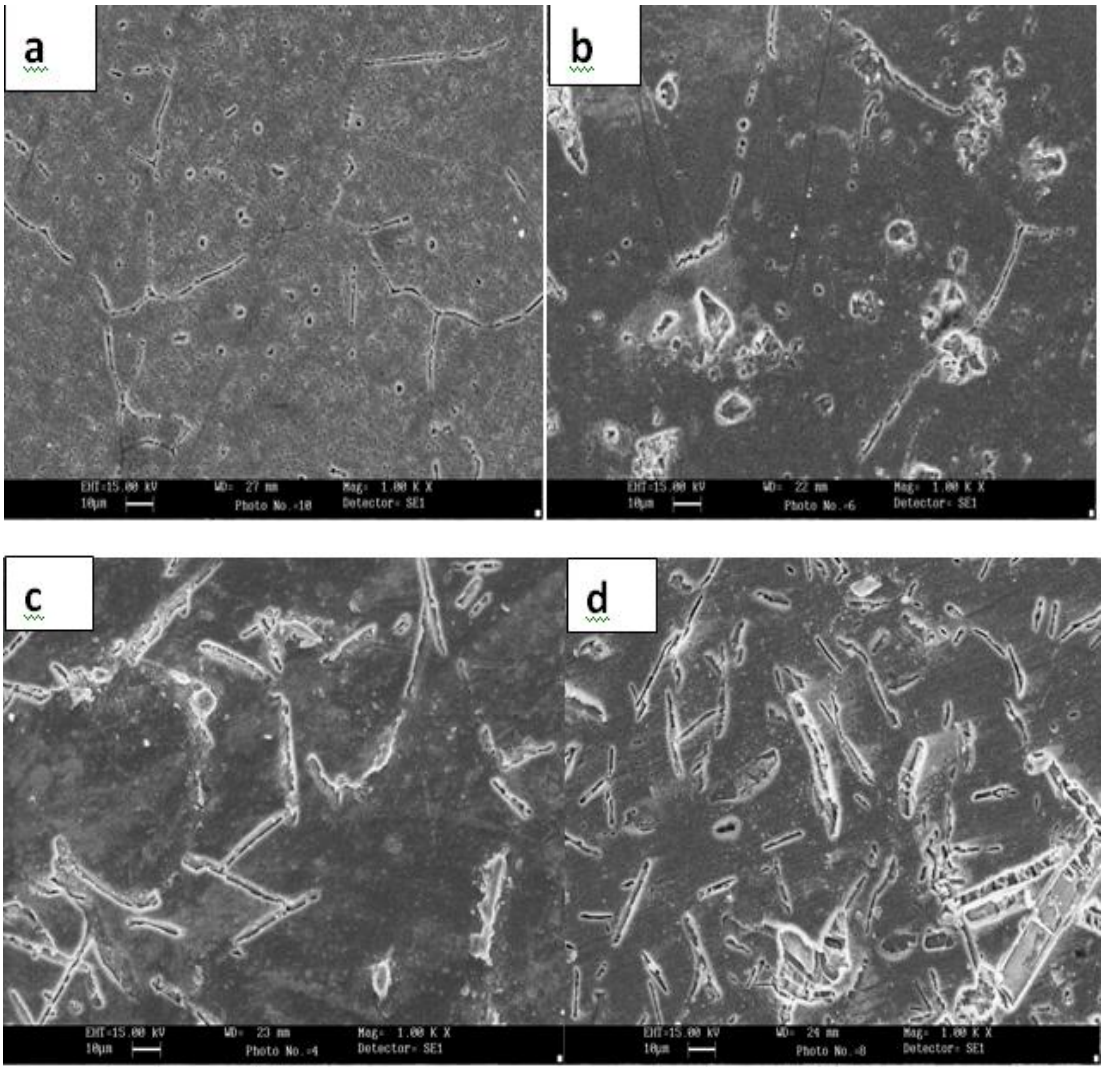

Figure 9: SEM micrographs of (a) Al-1.67%Fe (b) Al-3.36%Fe (c) Al-6.23%Fe (d) Al-11.2% Fe composite.

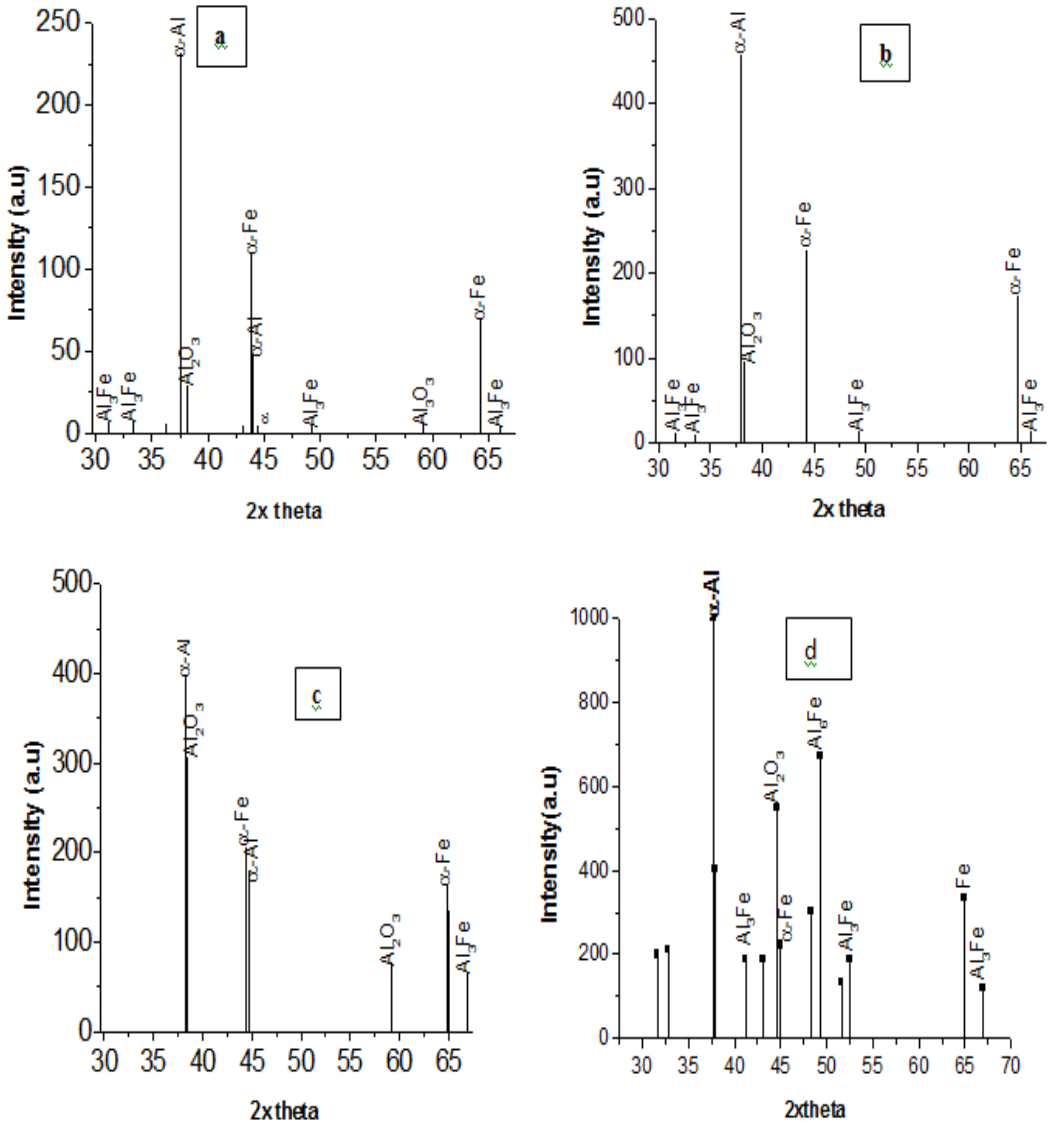

Figure 10: XRD graph of (a) Al-1.67%Fe (b) Al-3.36%Fe (c) Al-6.23%Fe (d) Al-11.2% Fe composite, showing presence of $FeAl_3$

-yielding an equilibrium $FeAl_3$ phase (shown in Figure 8a or 9a). But these are again confirmed from the XRD investigation. At the lower percentage of the iron in the matrix, the peak of $FeAl_3$ along with aluminum is present as shown in Figure 10a and b. But during casting aluminum gets oxidized to alumina. The XRD micrographs are also contained the peak of alumina.

When the concentration of the alloying additive (Fe) is increased from 2 to 9.5 at %, extremely rapid hardening yields a metastable crystallized intermetallic $FeAl_6$ phase in addition to the aluminum-base supersaturated solid solution. Iron in the aluminum forms an intermetallic compound such as $FeAl_3$ as shown in Figure 8 c and d.

Wear studies

The wear is the sliding phenomenon, in which the material is totally lost from the surface. The wear rate is calculated from the following formula:

$$\text{Wear rate} = \frac{loss\ of\ volume}{area\ x\ sliding\ distance}$$

The unit of wear rate in this case is m^3/m^3. The variation of bulk wear with sliding distance was studied at different combination of loads and velocities. Figure 11 shows results of bulk wear for a test conducted at 0.37 MPa load and 0.772 m/s sliding velocity. The bulk wear is computed in terms of only volume loss. It is seen that the initial running-in period is followed by steady state wear for all the composites. The bulk wear continuously decreases with increase in iron content.

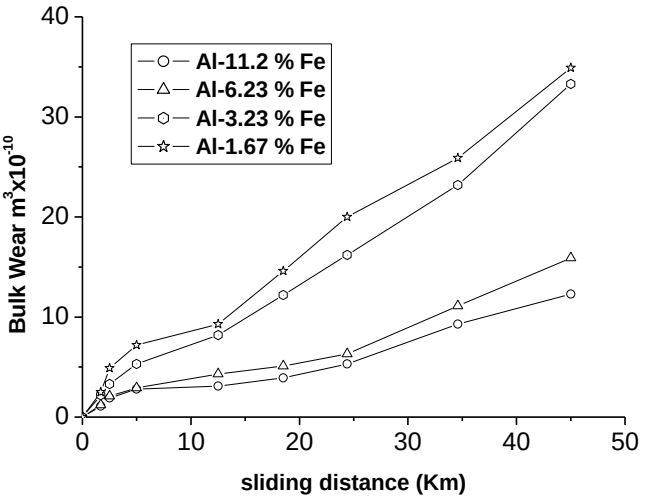

Figure 11: Variation of bulk wears with sliding distance at 3 kg load and 0.772 m/s sliding velocity for as-cast Al-Fe composites

Steady state wear is observed after initial running-in period of 500-1000m in almost all the case irrespective of load or sliding velocity used. Al-11.2 %Fe showed lower bulk wear among all the composite which may be due to higher amount of hard phase formation increasing the overall hardness of the composite material. The relation found here is in accordance with the pattern for most metallic materials derived theoretically as well as observed experimentally [24, 33]. However, at higher combination of load and sliding velocity bulk wear is higher for all the four composite.

The studies conducted to see the effect of applied load on wear rate reveled that wear rate increased continuously with load in a linear manner irrespective of the sliding velocity [5, 13] used as it is evident from Figure 12 at a particular velocity. Figure 13 shows the variation of wear rate with sliding velocity at 1kg load. Like other aluminum alloys/composite, Al-Fe composite showed an initial decrease in wear rate followed by a sharp increase in wear rate after attaining minima in wear rate for all the composites at different loads. But in all the case wear rate decrease with increase in iron content for all combination of loads and sliding velocities used [12, 19, 34]. Figure 14 a and b shows the SEM study of the wear track of Al-11.2 wt% Fe at a different load. Wear debris are also examined with SEM. Debris of Al-Fe composite at a distance of about 1430m shows mainly oxidative nature and wear track is smooth with thin oxide layer, however at a distance of about 40000m debris comprised of different oxides with metallic particle and wear track was observed with thick oxide layer with deeper track as shown in Figure 14 b.

The mechanistic approach is changed with change the velocity and load. In this case the sliding distance was kept constant i.e., 4000m. Due to examination of wear track and debris as shown in the Figure 15a and b, the oxidative -metallic to metallic is observed as applied load and sliding velocity. The oxide film is broken at the higher velocity and load and deep grove and elimination of surface is observed as shown in Figure 16 a and b.

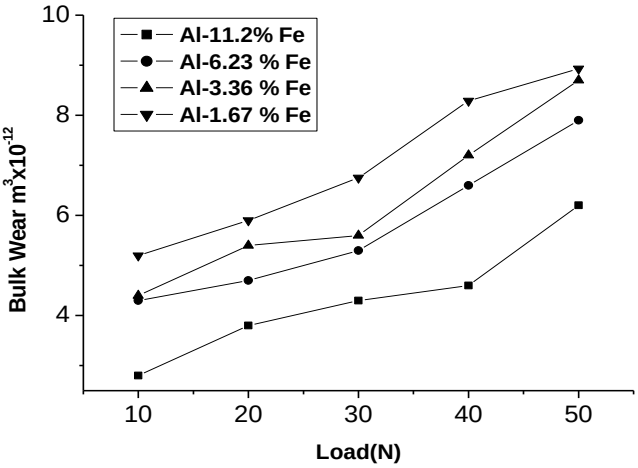

Figure 12.Variation of wear ate with load for Al-Fe composites

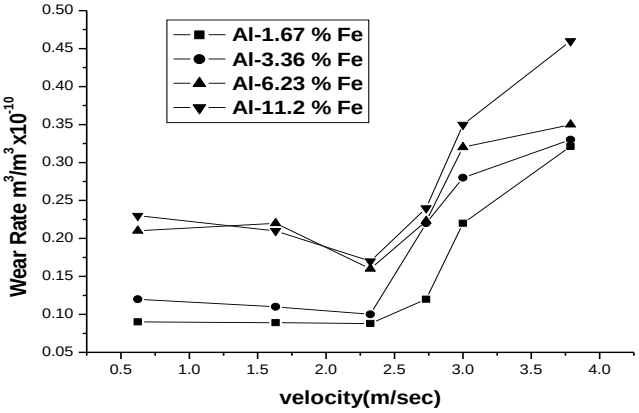

Figure 13.Variation of wear ate with sliding velocity at 1 kg load for Al-Fe composites.

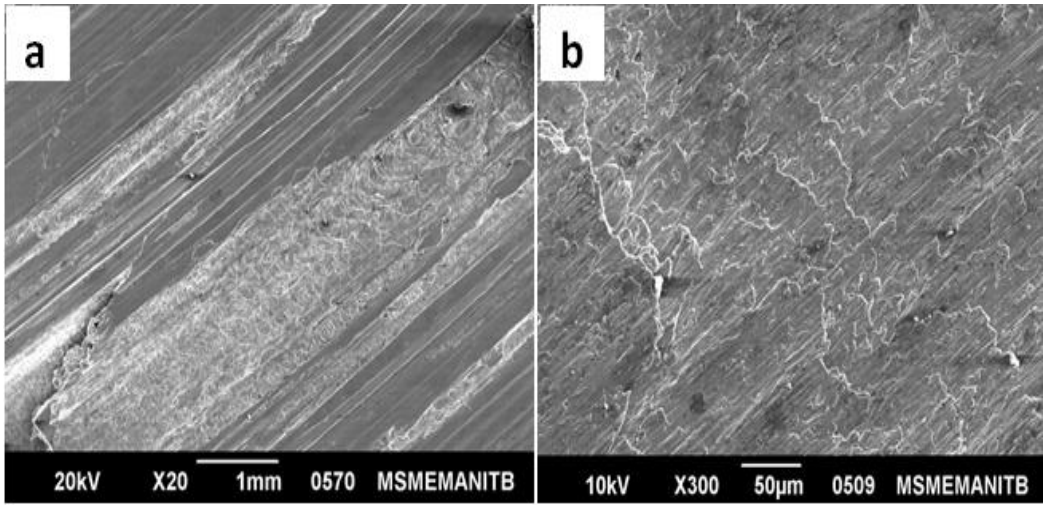

Figure 14: SEM micrographs of wear tracks of Al–11.2 wt. % Fe composite for 0.772 m/s sliding velocity and different sliding distance of (a) 1430m and (b) 4000m

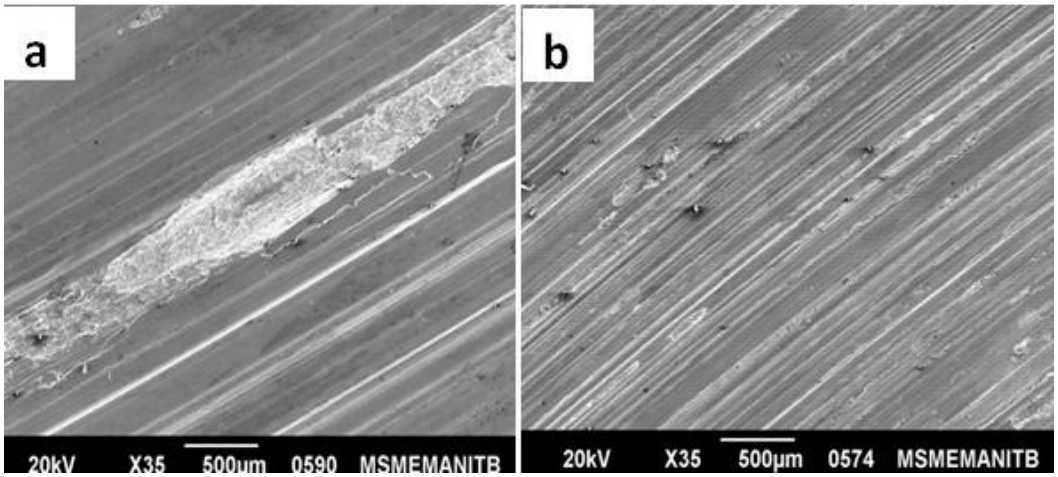

Figure 15: SEM micrographs of wear tracks of Al–11.2 wt. % Fe composite for 0.772 m/s sliding velocity and different loads of (a) 2.0 kg and (b) 5.0 kg.

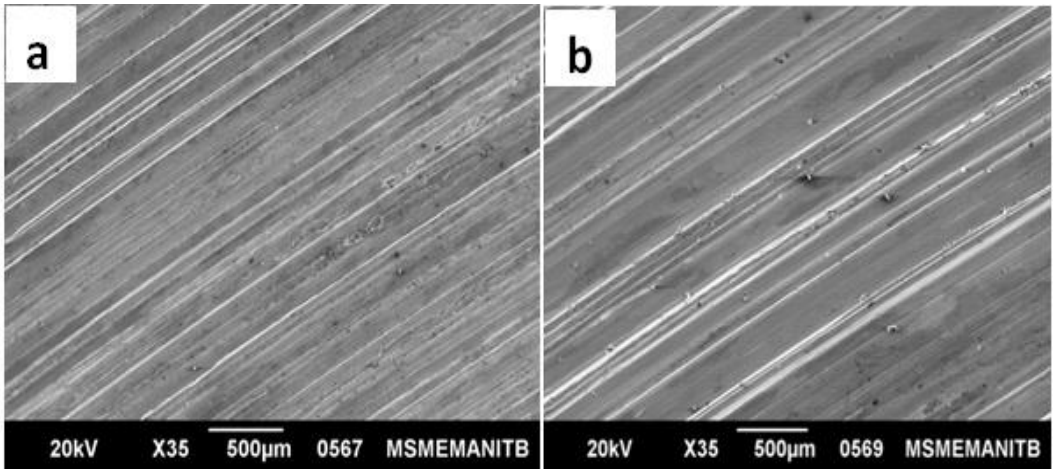

Figure 16: SEM micrographs of wear tracks of debris of Al–11.2 wt. % Fe composite for 3.24 m/s sliding velocity and different loads of (a) 2.0 kg and (b) 5.0 kg.

SEM images of the transverse section of the worn surface showed that the build up of oxide layer depending on sliding distance, composition, applied load and sliding velocity. In mild wear region after large sliding distance cracking and spalling of oxide layer is observed on the wear track which turns into deep groove after large sliding distance for all Al-Fe composite. The higher percentage of oxide layer is formed in sample with lower iron content in comparison to the samples of higher Fe-content. The oxidation of the worn surface depends upon the hardness of the materials. The hardness of the materials varies with iron content in the materials. Al-11.2% Fe shows the maximum hardness and they have capability to sustain the load. This increases the bulk hardness of composite from 95 to 179 VHN with iron percentage increase from 1.67 to 11.2%, hence improving the wear resistance of composites with increase in percentage iron for all case irrespective of load and sliding velocity.

XRD examination of wear debris shows the diffraction peaks corresponding to coexisting aluminum and alumina, different oxide of iron as well as the peaks of iron as shown in Figure 17. The main peak of the alumina are found at 37.6(hkl: 213) and 37.8^{o} (hkl: 109) and the different oxides of the iron at 33.18 and 35.46^{o}. The peak of the iron is present at 44.67^{o} [5].

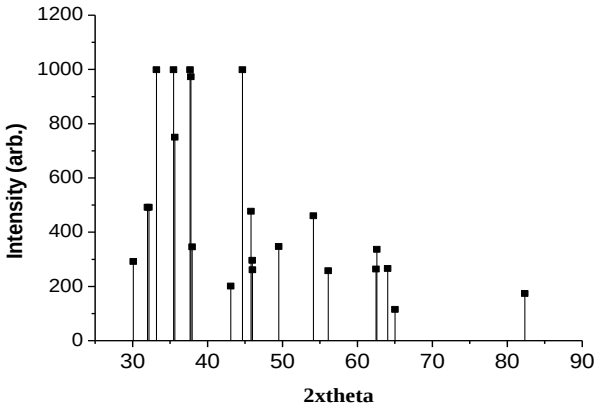

Figure 17: XRD plot of wear debris of Al–11.2 wt. % Fe composite at 0.772 m/s sliding velocity and 2.0 kg load

FRICTION STUDIES:

The character of friction variation with sliding at the specific load (i.e 10N) is illustrated in Figure 18. The fig shows is graphically representation of the results obtained from the friction experiment at a fixed load and sliding velocity. It is evident from the Figure 18 the friction coefficient drastically decreases during the running in period. During the steady state period the friction coefficient is being stabilized. The friction behavior also varies with applied load. The average value of the friction coefficient at normal load is shown in Figure 19. In accordance with the figure the increase of the friction coefficient corresponds to increase the normal load. The increase rate is especially evident for load change from 15 to 30 N.

Diagrams in Figure 20 show the dependence of the steady-state friction coefficient on the sliding speed, for various loads in dry sliding conditions. The nature of the dependence, in all the tested composite materials, manifests as decrease of the friction coefficient with increase of the sliding speed. The degree of change is especially prominent in the region of lower values of speeds [35].

The worn surfaces of the samples from the SEM examination are shown in Figure 21. The worn surfaces of the Al-11.2 wt% Fe samples were noticed to be smoother than those of the Al-1.67 wt %Fe. Generally, the parallel ploughing grooves and scratches can be seen over all the surfaces in the direction of sliding. These grooves and scratches resulted from the ploughing action of asperities on the counter disc of significantly higher hardness [36].

It can be noticed from the figure that for all the contact loads, the friction coefficient of Al-11.2%Fe is found to be low in comparsion to the other the composites. Al-11.2 wt% Fe showed higher hardness and from the metallographic observation indicated is uniformly distribution of $FeAl_3$ within the composite. The iron internetallic with aluminum has higher hardness and also bear the maximum load. Therefore it acts as lubricant in the materials. It bears maximum amount of the load due to formation of hard intermetallic from the solidification of the melts. Therefore it reduces the wear rate.

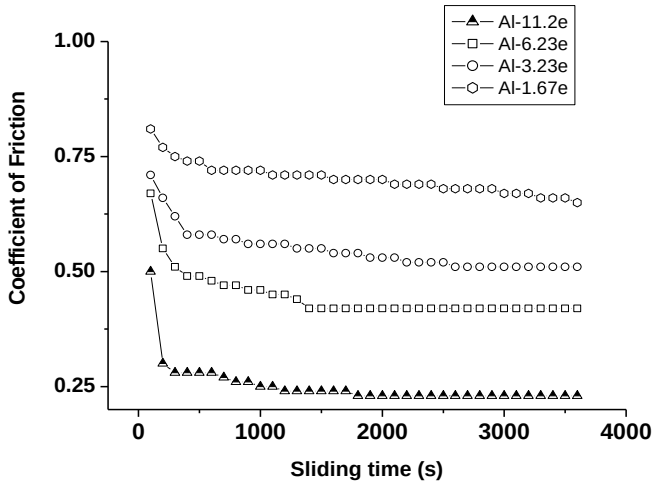

Figure18: Friction coefficient variation of Al-Fe composite during sliding time at fixed specific loads (i.e. 10N) and sliding speeds (4000m)

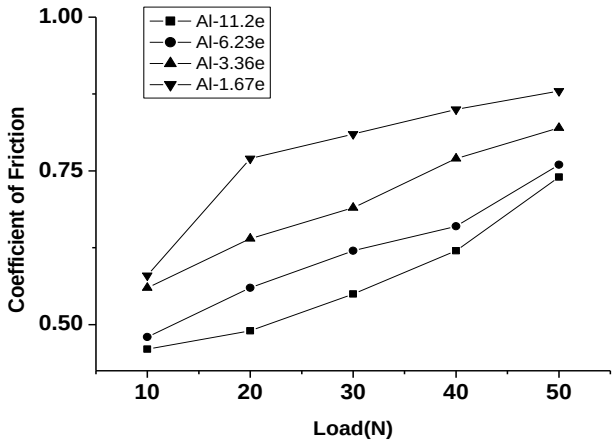

Figure 19: Coefficient of friction vs. applied load for Al-Fe composite at 0.932m/sec.

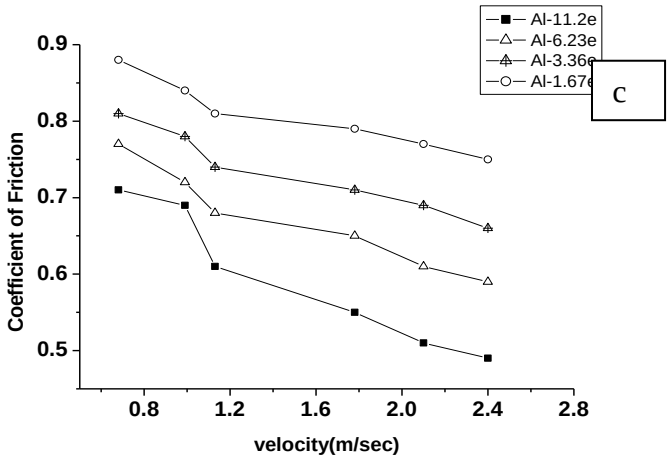

Figure 20: Friction coefficient vs. sliding speed of Al-Fe composite at different applied loads: 10N (b) 20N (c) 50N

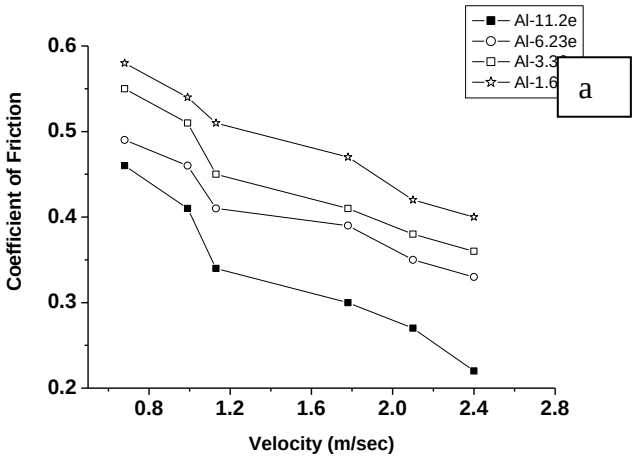

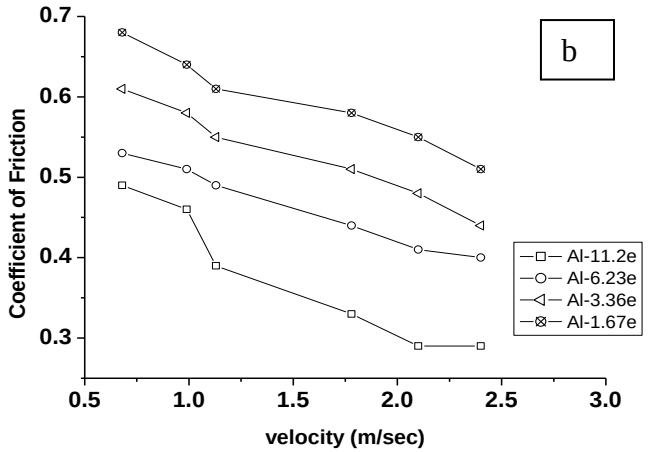

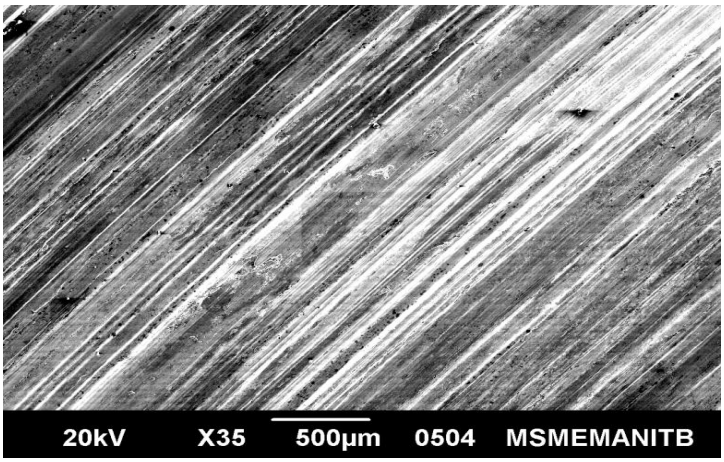

Figure 21: Worn surface of the Al-Fe composite tested in dry lubricated sliding condition for 50 N of applied load and 0.26 m/s of sliding speed during friction experiment.

IV. CONCLUSION

It can be observed from the present investigation that iron could be successfully and uniformly distributed in aluminum using impeller mixing chill casting technique. UTS, 0.2%PS and VHN increased with increase the volume fraction of the iron in the matrix. The Al-11.2%Fe composite showed higher percentage of elongation while compared to Al-6.23% Fe. Finally the increase in iron content in the matrix supports the formation of different type of intermetallic. This intermetallic increased with volume fraction of iron in the matrix. Wear rate with sliding distance showed almost linear relationship for fixed load and sliding velocities. Wear rate of the composite materials initially decrease with sliding velocity and attains a minima in wear rate and then increases with further increase in sliding velocity.

REFERENCES

[1] Patel A N. and Diamond S, *Mater. Sci. Eng.*, 1988, 98, 329.

[2] Pathak J P, Singh V and Tiwari S N, *J. Mater. Sci. Lett.*, 1992, **11**, 639.

[3] Massalki T B, *Binary Alloy Phase Diagrams* (American Society for Metals, Metals Park, OH, 1986).

[4] Ratke L and Diefenbach S, *Mat. Sci. Eng*., 1995, **R15**, 263.

[5] Singh R N and Sommer F, *Rep. Prog. Phys*., 1997, **60**, 57.

[6] García-Cordovilla C, Narciso J, and Louis E, *Wear*, 1996, **192**, 1-2, 170-177.

[7] Senkov O N, Froes F H, Stolyarov V V , Valiev R Z and Liu J, *Scr. Mater*., 1998, **38,** 1516.

[8] Zhang D L and Cantor B, *Acta Metall. Mater*., 1991, **39**, 1595.

[9] Tonejc A and Bonefasčié A, *Scr. Metall*., 1969, **3,** 145.

[10] Korkut M H, *Materials Science and Technology*, 2004, **20, (1)**, 73-81.

[11] Kattner U R and Massalski T B, "Al–Fe, binary alloy phase diagrams (ed.)" (Metals Park, Ohio: American Society for Metals), 1986, **Vol. 1**, p. 147.

[12] Yijie Z, Naiheng Ma, Hongzhan Yi, Wang S, and Wang H, *Materials and Design*, 2006, **27,** 794-798.

[13] Riontino G and Zanada A, *Mater. Sci. Eng. A*, 1994, **323,** 179–180.

[14] Badan B, Margini M and Zambon A, *Scr. Mater*., 1996, **13,** 35.

[15] Huang B, Tokizane N, Ishihara K N, Shingu P H and Nasu S, *J. Non-Cryst. Solids*, 1990, **688**, 117-118.

[16] Niu X P, Froyen L, Delaey L, and Peytour C, *J. Mater. Sci.*, 1994, **29** 3724

[17] Mukhopadhyay D K, Suryanarayana C, and Froes F H, *Metall. Mater. Trans. A* 1995, **26,** 1939.

[18] Fadeeva V I and Leonov A V, *Mater. Sci. Eng. A*, 1996, **206**, 90.

[19] Kaloshkin S D, Tcherdynstev V V, Tomlin A I, Gunderov D V, Stolyarov V V, Baldokhin Y V, Brodova G I, and Shelekhov E V, *Mater. Trans.* 2002, **JIM-43,** 2031.

[20] Rohatgi P, *AFS Trans*., 2001, 1–133.

[21] Ibrahim I A, Mohamed F A, and Lavernia E J, *J. Mater. Sci*., 1991, **26**, 1137–56.

[22] Lloyd D J, *Int. Mater. Rev*., 1994, **39 (1)**, 1–23.

[23] Ray S, *J. Mater. Sci*., 1993, **28**, 5397–5413.

[24] Miracle D B, *Compos. Sci. Technol*., 2005, **65**, 2526–40.

[25] Asthana R, *Adv. Perf. Mater*, 1998, **5**, pp. 213–55.

[26] Chawala N and Chawala K K, *J. Mater*., 2006, **58** (11), 67–70.

[27] Pouranvari M, Ekrami A, and Kokabi AN H, *J. Alloys Compd*., 2008, **461**, 641–47.

[28] Rao A K Prasada, K Das, Murty B S, and Chakraborty M, *Wear*, 2006, **261**, 133–39.

[29] Kori S A and Chandrashekharaiah T M, *Wear*, 2007, **263**, 745–55.

[30] Raadnui S, *Tribology International*, 2005, **38**(10), 871-878.

[31] Mandolfo L F, *Aluminum Alloys, structure and properties*, Butterworth's London, 1976, 8585

[32] Narayanasamy R, Selvakumar N, and Pandey K S, *Materials and Design* 2007, **28,** 1358-1363.

[33] Skrotzki W, Keegler K, Tamm R, and Oertel C G, *Cryst. Res. Technol*. 2005, **40**, 90-94.

[34] Miyajima T, and Iwai Y, *Wear*, 2003, **255**, 606-616.

[35] Zou X G, Miyahara H, Yamamoto K, and Ogi K, *Materials Science and Technology*, 2003, **19,** 1519-1526.

[36] Young R M K and Clyne T W, *Scr. Metall*., 1981, **15,** 1211.